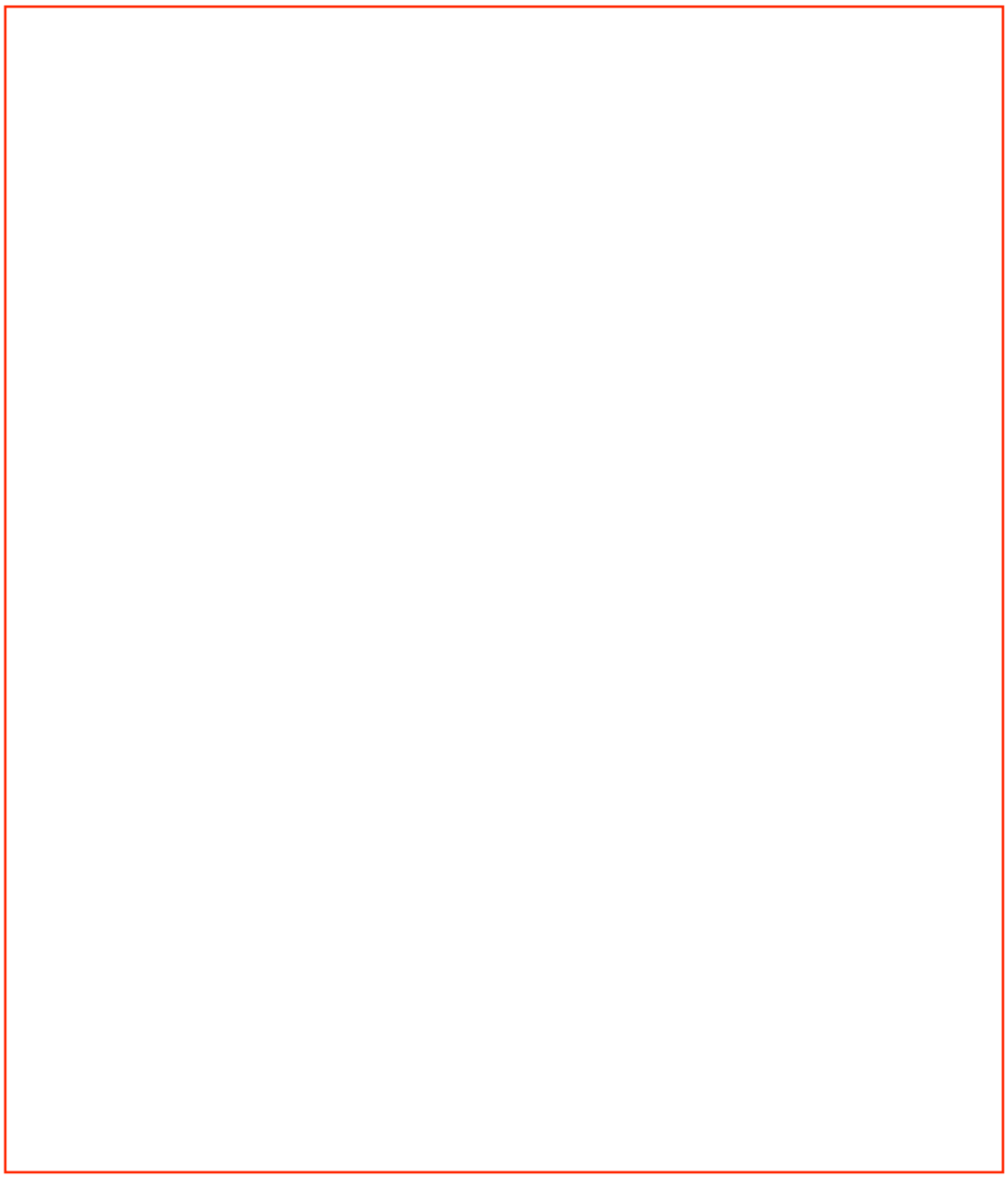

1.4.2 Quantum Rotor Model

We turn to the somewhat less familiar quantum rotor models. Elementary quantum rotors do not exist in nature; rather, each quantum rotor is an effective quantum degree of freedom for the low energy states of a small number of electrons or atoms. We will first define the quantum mechanics of a single rotor and then turn to the lattice quantum rotor model. The connection to the experimental models introduced in Section 1.3 will be

described below in Section 1.4.3. Further details of this connection appear in Chapters 9, 19.

Each rotor can be visualized as a particle constrained to move on the surface of a (fictitious) ($N > 1$)-dimensional sphere. The orientation of each rotor is represented by an N-component unit vector $\hat{\mathbf{n}}_i$ which satisfies

$$\hat{\mathbf{n}}^2 = 1. \tag{1.14}$$

The caret on $\hat{\mathbf{n}}_i$ reminds us that the orientation of the rotor is a quantum mechanical operator, while i represents the site on which the rotor resides; we will shortly consider an infinite number of such rotors residing on the sites of a d-dimensional lattice. Each rotor has a momentum $\hat{\mathbf{p}}_i$, and the constraint (1.14) implies that this must be tangent to the surface of the N-dimensional sphere. The rotor position and momentum satisfy the usual commutation relations

$$[\hat{n}_\alpha, \hat{p}_\beta] = i\delta_{\alpha\beta} \tag{1.15}$$

on each site i; here $\alpha, \beta = 1 \ldots N$. (Here, and in the remainder of the book, we will always measure time in units in which

$$\hbar = 1, \tag{1.16}$$

unless stated explicitly otherwise. This is also a good point to note that we will also set Boltzmann's constant

$$k_B = 1 \tag{1.17}$$

by absorbing it into the units of temperature, T.) We will actually find it more convenient to work with the $N(N-1)/2$ components of the rotor angular momentum

$$\hat{L}_{\alpha\beta} = \hat{n}_\alpha \hat{p}_\beta - \hat{n}_\beta \hat{p}_\alpha. \tag{1.18}$$

These operators are the generators of the group of rotation in N dimensions, denoted O(N). Their commutation relations follow straightforwardly from (1.15) and (1.18). The case $N = 3$ will be of particular interest to us: For this we define $\hat{L}_\alpha = (1/2)\epsilon_{\alpha\beta\gamma} L_{\beta\gamma}$ (where $\epsilon_{\alpha\beta\gamma}$ is a totally antisymmetric tensor with $\epsilon_{123} = 1$), and then the commutation relation between the operators on each site are

$$\begin{aligned} [\hat{L}_\alpha, \hat{L}_\beta] &= i\epsilon_{\alpha\beta\gamma}\hat{L}_\gamma, \\ [\hat{L}_\alpha, \hat{n}_\beta] &= i\epsilon_{\alpha\beta\gamma}\hat{n}_\gamma, \\ [\hat{n}_\alpha, \hat{n}_\beta] &= 0; \end{aligned} \tag{1.19}$$

the operators with different site labels all commute.

The dynamics of each rotor is governed simply by its kinetic energy term; interesting effects will arise from potential energy terms that couple the rotors together, and these will be considered momentarily. Each rotor has the kinetic energy

$$H_K = \frac{J\tilde{g}}{2}\hat{\mathbf{L}}^2, \tag{1.20}$$

where $1/J\tilde{g}$ is the rotor moment of inertia (we have put a tilde over g as we wish to reserve g for a different coupling to be introduced below). The Hamiltonian H_K can be readily diagonalized for general values of N by well-known group theoretical methods. We quote the results for the physically important cases of $N = 2$ and 3. For $N = 2$ the eigenvalues are

$$J\tilde{g}\ell^2/2 \qquad \ell = 0, 1, 2, \ldots; \quad \text{degeneracy} = 2 - \delta_{\ell,0}. \tag{1.21}$$

Note that there is a nondegenerate ground state with $\ell = 0$, while all excited states are two-fold degenerate, corresponding to a left- or right-moving rotor. This spectrum will be important in the mapping to physical models to be discussed in Section 1.4.3. For $N = 3$, the eigenvalues of H_K are

$$J\tilde{g}\ell(\ell+1)/2 \qquad \ell = 0, 1, 2, \ldots; \quad \text{degeneracy} = 2\ell + 1, \tag{1.22}$$

corresponding to the familiar angular momentum states in three dimensions. These states can be viewed as representing the eigenstates of an even number of antiferromagnetically coupled Heisenberg spins, as will be discussed more explicitly in Section 1.4.3 and in Chapter 19, where will see that there is a general and powerful correspondence between quantum antiferromagnets and $N = 3$ rotors.

We are ready to write down the full quantum rotor Hamiltonian, which shall be the focus of intensive study in Parts II and III. We place a single quantum rotor on the sites, i, of a d-dimensional lattice, obeying the Hamiltonian

$$H_R = \frac{J\tilde{g}}{2}\sum_i \hat{\mathbf{L}}_i^2 - J\sum_{\langle ij\rangle} \hat{\mathbf{n}}_i \cdot \hat{\mathbf{n}}_j. \tag{1.23}$$

We have augmented the sum of kinetic energies of each site with a coupling, J, between rotor orientations on neighboring sites. This coupling energy is minimized by the simple "magnetically ordered" state in which all the rotors are oriented in the same direction. In contrast, the rotor kinetic energy is minimized when the orientation of the rotor is maximally uncertain (by the uncertainty principle), and so the first term in H_R prefers a quantum paramagnetic state in which the rotors do not have a definite orientation (i.e., $\langle \mathbf{n} \rangle = 0$). Thus the roles of the two terms in H_R closely parallel those

of the terms in the Ising model H_I. As in Section 1.4.1, for $\tilde{g} \gg 1$, when the kinetic energy dominates, we expect a quantum paramagnet in which, following (1.9),

$$\langle 0|\hat{\mathbf{n}}_i \cdot \hat{\mathbf{n}}_j|0\rangle \sim e^{-|x_i - x_j|/\xi}. \tag{1.24}$$

Similarly, for $\tilde{g} \ll 1$, when the coupling term dominates, we expect a magnetically ordered state in which, as in (1.12),

$$\lim_{|x_i - x_j| \to \infty} \langle 0|\hat{\mathbf{n}}_i \cdot \hat{\mathbf{n}}_j|0\rangle = N_0^2. \tag{1.25}$$

Finally, we can anticipate a second-order quantum phase transition between the two phases at $\tilde{g} = \tilde{g}_c$, and the behavior of N_0 and ξ upon approaching this point will be similar to that in the Ising case. These expectations turn out to be correct for $d > 1$, but we will see that they need some modifications for $d = 1$. In one dimension, we will show that $\tilde{g}_c = 0$ for $N \geq 3$, and so the ground state is a quantum paramagnetic state for all nonzero $\tilde{g}$. The case $N = 2$, $d = 1$ is special: There is a transition at a finite $\tilde{g}_c$, but the divergence of the correlation length does not obey (1.2) and the long-distance behavior of the correlation function $\tilde{g} < \tilde{g}_c$ differs from (1.25). This case will not be considered until Section 20.3 in Part III.

1.4.3 Physical realizations of quantum rotors

We will consider the $N = 3$ quantum rotors first, and expose a simple and important connection between O(3) quantum rotor models and a certain class of "dimerized" antiferromagnets, of which $TlCuCl_3$ is the example we highlighted in Section 1.3. Actually the connection between rotor models and antiferromagnets is far more general than the present discussion may suggest, as we will see later in Chapter 19. However, this discussion should enable the reader to gain an intuitive feeling for the physical interpretation of the degrees of freedom of the rotor model.

Consider a dimerized system of "Heisenberg spins" $\hat{\mathbf{S}}_{1i}$ and $\hat{\mathbf{S}}_{2i}$, where i now labels a pair of spins (a 'dimer'). Their Hamiltonian is

$$H_d = K \sum_i \hat{\mathbf{S}}_{1i} \cdot \hat{\mathbf{S}}_{2i} + J \sum_{\langle ij \rangle} \left(\hat{\mathbf{S}}_{1i} \cdot \hat{\mathbf{S}}_{1j} + \hat{\mathbf{S}}_{2i} \cdot \hat{\mathbf{S}}_{2j} \right). \tag{1.26}$$

The $\hat{\mathbf{S}}_{ni}$ ($n = 1, 2$ labels the spins within a dimer) are spin operators usually representing the total spin of a set of electrons in some localized atomic states. See Fig 1.3. On each site, the spins $\hat{\mathbf{S}}_{ni}$ obey the angular momentum

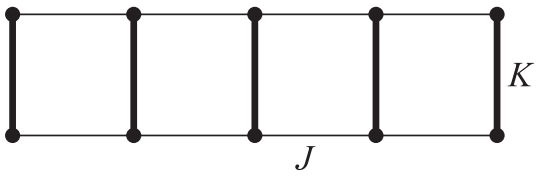

Figure 1.3 A dimerized quantum spin system. Spins with angular momentum S reside on the circles, with antiferromagnetic exchange couplings as shown.

commutation relations

$$\left[\hat{S}_\alpha, \hat{S}_\beta\right] = i\epsilon_{\alpha\beta\gamma}\hat{S}_\gamma \tag{1.27}$$

(the site index has been dropped above), while spin operators on different sites commute. These commutation relations are the same as those of the $\hat{\mathbf{L}}$ operators in (1.19). However, there is one crucial difference between Hilbert space of states on which the quantum rotors and Heisenberg spins act. For the rotor models we allowed states with arbitrary total angular momentum ℓ on each site, as in (1.22), and so there were an infinite number of states on each site. For the present Heisenberg spins, however, we will only allow states with total spin S on each site, and we will permit S to be integer or half-integer. Thus there are precisely $2S + 1$ states on each site

$$|S, m\rangle \quad \text{with } m = -S \ldots S, \tag{1.28}$$

and the operator identity

$$\hat{\mathbf{S}}_{ni}^2 = S(S+1) \tag{1.29}$$

holds for each i and n. In addition to describing $TlCuCl_3$, Hamiltonians like H_d describe spin-ladder compounds in $d = 1$ [39, 131] and "double layer" antiferromagnets in the family of the high-temperature superconductors in $d = 2$ [581, 582, 387, 402, 517, 518, 159].

Let us examine the properties of H_d in the limit $K \gg J$. As a first approximation, we can neglect the J couplings entirely, and then H_d splits into decoupled pairs of sites, each with a strong antiferromagnetic coupling K between two spins. The Hamiltonian for each pair can be diagonalized by noting that $\mathbf{S}_{1i}$ and $\mathbf{S}_{2i}$ couple into states with total angular momentum $0 \le \ell \le 2S$, and so we obtain the eigenenergies

$$(K/2)(\ell(\ell+1) - 2S(S+1)), \qquad \text{degeneracy } 2\ell + 1. \tag{1.30}$$

Note that these energies and degeneracies are in one-to-one correspondence with those of a single quantum rotor in (1.22), apart from the difference

that the upper restriction on ℓ being smaller than $2S$ is absent in the rotor model case. If one is interested primarily in low energy properties, then it appears reasonable to represent each pair of spins by a quantum rotor.

We have seen that the $K/J \to \infty$ limit of H_d closely resembles the $\tilde{g} \to \infty$ limit of H_R. To first order in $\tilde{g}$, we can compare the matrix elements of the term proportional to J in H_R among the low-lying states, with those of the J term in H_d; it is not difficult to see that these matrix elements become equal to each other for an appropriate choice of couplings: see exercise 6.6.1. Therefore we may conclude that the low-energy properties of the two models are closely related for large K/J and $\tilde{g}$. Somewhat different considerations in Chapter 19 will show that the correspondence also applies to the quantum critical point and to the magnetically ordered phase.

The main lesson of the above analysis is that the O(3) quantum rotor model represents the low energy properties of quantum antiferromagnets of Heisenberg spins, with each rotor being an effective representation of a *pair* of antiferromagnetically coupled spins. The strong-coupling spectra clearly indicate the operator correspondence $\hat{\mathbf{L}}_i = \hat{\mathbf{S}}_{1i} + \hat{\mathbf{S}}_{2i}$, and so the rotor angular momentum represents the total angular momentum of the underlying spin system. Examination of matrix elements in the large-S limit shows that $\hat{\mathbf{n}}_i \propto \hat{\mathbf{S}}_{1i} - \hat{\mathbf{S}}_{2i}$: the rotor coordinate $\hat{\mathbf{n}}_i$ is the antiferromagnetic order parameter of the spin system. Magnetically ordered states of the rotor model with $\langle \hat{\mathbf{n}}_i \rangle \neq 0$, which we will encounter below, are therefore spin states with long-range antiferromagnetic order and have a vanishing total ferromagnetic moment. Quantum Heisenberg spin systems with a net ferromagnetic moment are *not* modeled by the quantum rotor model (11.1) – these will be studied in Section 19.2 by a different approach.

6

The quantum rotor model

This chapter will analyze the spectrum of the quantum rotor model (1.25), whose Hamiltonian we reproduce here

$$H_R = \frac{J\tilde{g}}{2} \sum_i \hat{\mathbf{L}}_i^2 - J \sum_{\langle ij \rangle} \hat{\mathbf{n}}_i \cdot \hat{\mathbf{n}}_j. \tag{6.1}$$

Our analysis will parallel that of the quantum Ising model in Chapter 10. We will begin by a perturbative analysis of both phases: the paramagnetic phase at $\tilde{g} \gg 1$, and the magnetically ordered phase at $\tilde{g} \ll 1$. We will then describe the mapping of the partition function of the quantum rotor model in d dimensions to the classical O(N) spin model in (2.3) and (3.2). This mapping will allow us to address the vicinity of the critical point using the methods of Chapters 3 and 4.

We will begin with the perturbative analyses, which are expected to hold on either side of a quantum critical point at $\tilde{g} = \tilde{g}_c$, which separates the ordered and the quantum paramagnetic phases. We will see later that $\tilde{g}_c = 0$ in $d = 1$, but $\tilde{g}_c > 0$ for $d > 1$.

6.1 Large $\tilde{g}$ expansion

The strong-coupling expansion was discussed in Ref. [202] and briefly noted in Section 1.4.2. At $\tilde{g} = \infty$, the exchange term in H_R can be neglected, and the Hamiltonian decouples into independent sites and can be diagonalized exactly. The eigenstates on each site are the eigenstates of $\mathbf{L}^2$; for $N = 3$ these are the states of (1.24):

$$|\ell, m\rangle_i \quad \ell = 0, 1, 2, \ldots, \quad -\ell \leq m \leq \ell \tag{6.2}$$

and have eigenenergy $J\tilde{g}\ell(\ell+1)/2$. The ground state of H_R in the large-$\tilde{g}$ limit consists of the quantum paramagnetic state with $\ell = 0$ on every site:

$$|0\rangle = \prod_i |\ell = 0, m = 0\rangle_i. \tag{6.3}$$

Compare this with the strong-coupling ground state (1.9) of the Ising model. Indeed, the remainder of the large g analysis of the quantum Ising model in Section 5.2 can be borrowed here for the rotor model, and we can therefore be quite brief. The lowest excited state is a "particle" in which a single site has $\ell = 1$, and this excitation hops from site to site. An important difference from the Ising model is that this particle is three-fold degenerate, corresponding to the three allowed values $m = -1, 0, 1$. The single-particle states are labeled by a momentum k and an azimuthal angular momentum m and have energy

$$\varepsilon_{\vec{k},m} = J\tilde{g}\left(1 - (2/3\tilde{g})\sum_\mu \cos(k_\mu a) + \mathcal{O}(1/\tilde{g}^2)\right) \tag{6.4}$$

where the sum over μ extends over the d spatial directions. This result is the analog of (5.8). Multi-particle states can be analyzed as in Section 5.2, with the only change being that the states and the S-matrices now carry $\mathrm{O}(N)$ indices.

6.2 Small $\tilde{g}$ expansion

For small $\tilde{g}$, the ground state breaks $\mathrm{O}(N)$ symmetry, and all the $\hat{\mathbf{n}}_i$ vectors orient themselves in a common, but arbitrary direction. This is similar to the broken Z_2 symmetry of the quantum Ising model in Section 5.3.

Excitations above this state consist of "spin waves," which can have an arbitrarily low energy (*i.e.*, they are "gapless"). This is a crucial difference from the Ising model in Section 5.3, in which there was an energy gap above the ground state. The presence of gapless spin excitations is a direct consequence of the continuous $\mathrm{O}(N)$ symmetry of H_R: We can make very slow deformations in the orientation of $\langle\hat{\mathbf{n}}\rangle$, obtaining an orthogonal state whose energy is arbitrarily close to that of the ground state. Explicitly, for $N = 3$, and a ground state polarized along $(0, 0, 1)$ we parameterize

$$\hat{\mathbf{n}}(x,t) = \left(u_1(x,t), u_2(x,t), \left(1 - u_1^2 - u_2^2\right)^{1/2}\right), \tag{6.5}$$

where $|u_1|, |u_2| \ll 1$. In this limit, the commutation relations (1.21) become

$$[\hat{L}_1, u_2] = i \quad , \quad [\hat{L}_2, u_1] = -i \tag{6.6}$$

i.e., u_1, $\hat{L}_2$ and u_2, $-\hat{L}_1$ are canonically conjugate pairs. Also, in the limit where $u_{1,2}$ are small, the rotor momenta are also in the $1,2$ plane, and hence the third component of the rotor angular momentum is negligibly small, $\hat{L}_3 \approx 0$; so by (1.21), $\hat{L}_1$ and $\hat{L}_2$ are commuting variables. We now insert (6.5) into (6.1), and focus on the long wavelength excitations by taking the continuum limit: this yields the Hamiltonian

$$H_R = \int \frac{d^d x}{a^d} \left[\frac{J\tilde{g}}{2} \left(\hat{L}_1^2 + \hat{L}_2^2 \right) + \frac{Ja^2}{2} \left((\nabla u_1)^2 + (\nabla u_2)^2 \right) \right], \tag{6.7}$$

where a is the lattice spacing. The reader will now recognize that (6.7) and the commutation relations (6.6) define the dynamics of a set of harmonic oscillators, 2 for each wavevector k. Explicitly, let us make the following normal mode expansion in terms of the harmonic oscillator creation and annihilation operators

$$\begin{aligned} u_\lambda(x) &= \int \frac{d^d k}{(2\pi)^d} \frac{J\tilde{g}}{\sqrt{2a^d \varepsilon_k}} \left(a_\lambda(k) e^{i\vec{k}\cdot\vec{x}} + a_\lambda^\dagger(\vec{k}) e^{-i\vec{k}\cdot\vec{x}} \right), \\ \epsilon_{\lambda\lambda'} L_{\lambda'}(x) &= -i \int \frac{d^d k}{(2\pi)^d} \sqrt{\frac{a^d \varepsilon_k}{2J\tilde{g}}} \left(a_\lambda(\vec{k}) e^{i\vec{k}\cdot\vec{x}} - a_\lambda^\dagger(\vec{k}) e^{-i\vec{k}\cdot\vec{x}} \right), \end{aligned} \tag{6.8}$$

where $\lambda = 1,2$ is a polarization index, $\epsilon_{\lambda\lambda'}$ is the unit antisymmetric tensor. Then it can be verified that if the $a(\vec{k},t)$ operators satisfy the familiar harmonic oscillator equal-time commutation relations

$$\begin{aligned} \left[a_\lambda(\vec{k}), a_{\lambda'}^\dagger(\vec{k}') \right] &= \delta_{\lambda\lambda'} (2\pi)^d \delta^d(\vec{k} - \vec{k}'), \\ \left[a_\lambda(\vec{k}), a_{\lambda'}(\vec{k}') \right] &= 0, \end{aligned} \tag{6.9}$$

the commutation relations (6.6) are obeyed. Further, the Hamiltonian explicitly displays the simple sum over independent harmonic oscillators

$$H_R = \sum_\lambda \int \frac{d^d k}{(2\pi)^d} \varepsilon_k \left[a_\lambda^\dagger(\vec{k}) a_\lambda(\vec{k}) + 1/2 \right]. \tag{6.10}$$

Here the oscillation frequency is

$$\varepsilon_k = ck \quad ; \quad c = Ja\sqrt{\tilde{g}}, \tag{6.11}$$

where c is the spin-wave velocity.

Thus the excitation spectrum of the magnetically ordered phase consists of 2 polarizations of quantized spin waves with dispersion $\varepsilon_k = ck$; for general N, there are $N-1$ spin waves. It is useful to recall how quantization of electromagnetic waves led to the concept of a particle-like excitation called

the photon: the particle is just a wavepacket. Similarly, here we can interpret the quantized spin waves as a set of $N-1$ quantized particles.

The reader should note the distinction between the $N-1$ particles in the ordered phase with the N particles obtained in the quantum paramagnet in the strong coupling expansion above. In the ordered phase, rotations about the axis of $\langle \hat{\mathbf{n}} \rangle$ do not produce a new state, and so there are only $N-1$ independent rotations about axes orthogonal to $\langle \hat{\mathbf{n}} \rangle$ that lead to gapless spin-wave modes.

The ground state wavefunction of the magnetically ordered state includes quantum zero-point motion of the spin waves about the fully polarized state. One consequence of the zero-point motion is that the ordered moment on each site is reduced at order $\tilde{g}$:

$$\begin{aligned} \langle \hat{n}_3 \rangle &= \left\langle (1 - u_1^2 - u_2^2)^{1/2} \right\rangle \\ &\approx 1 - (1/2) \left\langle u_1^2 + u_2^2 \right\rangle \\ &= 1 - \frac{\sqrt{\tilde{g}} a^{d-1}}{2} \int \frac{d^d k}{(2\pi)^d} \frac{1}{k}. \end{aligned} \tag{6.12}$$

In the last step we have evaluated the expectation value in the quantized harmonic oscillator ground state after using the normal mode expansion (6.8). The integral over momenta k is cut off at large k by the inverse lattice spacing, but there is no cutoff at small k. We therefore notice a small k divergence in $d = 1$, indicating an instability in the small-$\tilde{g}$ expansion. We will see that the small-$\tilde{g}$ prediction of a state with magnetic long-range order is never valid in $d = 1$, and the physical picture of the quantum paramagnet introduced by the large-$\tilde{g}$ expansion holds for all $\tilde{g}$. In contrast, the small-$\tilde{g}$ expansion appears stable for $d > 1$, and we do expect magnetically ordered states to exist. In this case, comparison of the small- and large-$\tilde{g}$ expansions correctly suggests the existence of a quantum phase transition at intermediate $\tilde{g}$.

The above was an analysis in the linearized, harmonic limit. The nonlinearities neglected above lead to nonzero spin-wave scattering amplitudes, which we will show later are quite innocuous at low enough energies in dimensions $d > 1$. Precisely in $d = 1$, spin-wave interactions are very important and destroy the long-range order of the ground state, as was already apparent from (6.12). For the classical ferromagnet (3.2), to which the present model maps, this corresponds to the absence of long-range order in $D = 2$ and is known as the Hohenberg–Mermin–Wagner theorem.

6.3 The classical XY chain and an O(2) quantum rotor

We will consider the $D = 1$, $N = 2$ classical ferromagnet; this is also referred to as the XY ferromagnet. We generalize (5.22) and (5.23) to $N = 2$ by replacing σ_ℓ^z by a two-component unit-length variable $\mathbf{n}_\ell$. This modifies (5.22) to

$$\mathcal{Z} = \prod_\ell \int D\mathbf{n}_i \delta\left(\mathbf{n}_\ell^2 - 1\right) \exp\left(-H\right); \tag{6.13}$$

for H we modify (5.23) to

$$H = -K \sum_{\ell=1}^{M_\tau} \mathbf{n}_\ell \cdot \mathbf{n}_{\ell+1} - \sum_{\ell=1}^{M_\tau} \mathbf{h} \cdot \mathbf{n}_\ell, \tag{6.14}$$

where, as in the Ising case, we have added a uniform field $\mathbf{h} = (h, 0)$. It is convenient to parameterize the unit-length classical spins, $\mathbf{n}_\ell$, by

$$\mathbf{n}_\ell = (\cos\theta_\ell, \sin\theta_\ell), \tag{6.15}$$

where the continuous angular variables θ_ℓ, run from 0 to 2π. In these variables, H takes the form

$$H = -K \sum_{\ell=1}^{M_\tau} \cos(\theta_\ell - \theta_{\ell+1}) - h \sum_{\ell=1}^{M_\tau} \cos\theta_\ell, \tag{6.16}$$

and the partition function is

$$\mathcal{Z} = \int_0^{2\pi} \prod_{\ell=1}^{M_\tau} \frac{d\theta_\ell}{2\pi} \exp(-H). \tag{6.17}$$

We again assume periodic boundary conditions with $\theta_{M_\tau+1} \equiv \theta_1$. Notice that in zero field, H remains invariant if all the spins are rotated by the same angle ϕ, $\theta_\ell \to \theta_\ell + \phi$, and so our results will not depend upon the particular orientation chosen for $\mathbf{h}$. The partition function can be evaluated by transfer matrix methods [149, 258] quite similar to those used for the Ising chain. Although we will not use such a method to obtain our results, we nevertheless describe the main steps for completeness. First write $\mathcal{Z}$ in the form

$$\begin{aligned} \mathcal{Z} &= \int_0^{2\pi} \prod_{i=1}^{M_\tau} \frac{d\theta_\ell}{2\pi} \langle\theta_1|\hat{T}|\theta_2\rangle\langle\theta_2|\hat{T}|\theta_3\rangle \cdots \langle\theta_{M_\tau}|\hat{T}|\theta_1\rangle \\ &= \mathrm{Tr}\hat{T}_\tau^M, \end{aligned} \tag{6.18}$$

where the symmetric transfer matrix operator $\hat{T}$ is defined by

$$\langle\theta|\hat{T}|\theta'\rangle = \exp\left(K\cos(\theta-\theta') + \frac{h}{2}(\cos\theta+\cos\theta')\right), \tag{6.19}$$

and the trace is clearly over continuous angular variable θ. As in the Ising case, we have to diagonalize the transfer matrix $\hat{T}$ by solving the eigenvalue equation

$$\int_0^{2\pi}\frac{d\theta'}{2\pi}\langle\theta|\hat{T}|\theta'\rangle\Psi_\mu(\theta') = \lambda_\mu\Psi_\mu(\theta) \tag{6.20}$$

for the eigenfunctions $\Psi_\mu(\theta)$ (with $\Psi_\mu(\theta+2\pi)=\Psi_\mu(\theta)$) and corresponding eigenvalues λ_μ. Then the partition function $\mathcal{Z}$ is simply

$$\mathcal{Z} = \sum_\mu \lambda_\mu^{M_\tau}, \tag{6.21}$$

where the sum extends over the infinite number of eigenvalues λ_μ. The solution of (6.20) is quite involved, and the present approach is a rather convoluted method of obtaining the universal properties of H.

Instead, it is useful to approach the problem with a little physical insight and take the scaling limit at the earliest possible stage. We anticipate, from our experience with the Ising model, that the universal scaling behavior will emerge at large values of K. For this case, θ_ℓ is not expected to vary much from one site to the next, suggesting that it should be useful to expand in terms of gradients of θ_ℓ. So we define a continuous coordinate $\tau = \ell a$, where a is the lattice spacing, and the label τ anticipates its eventual interpretation as the imaginary time coordinate of a quantum problem. Then, to lowest order in the gradients of the function $\theta(\tau=\ell a)\equiv\theta_\ell$, the Hamiltonian H takes the continuum form H_c:

$$H_c[\theta(\tau)] = \int_0^{L_\tau} d\tau\left[\frac{\xi}{4}\left(\frac{d\theta(\tau)}{d\tau}\right)^2 - \tilde{h}\cos\theta(\tau)\right], \tag{6.22}$$

where

$$\xi = 2Ka, \quad \tilde{h} = \frac{h}{a}, \tag{6.23}$$

and as before $L_\tau = M_\tau a$. The coefficient of the gradient squared term is clearly a length (along the time direction) and we have written this length in terms of the symbol ξ: The parameterization anticipates some of our subsequent results where we will see that ξ is the $h=0$ correlation length of an infinite XY chain. With this new form of H, the partition function

becomes a functional integral

$$\mathcal{Z}_c = \sum_{p=-\infty}^{\infty} \int_{\theta(L_\tau)=\theta(0)+2\pi p} \mathcal{D}\theta(\tau) \exp\left(-H_c[\theta(\tau)]\right). \tag{6.24}$$

The integral is taken over all functions $\theta(\tau)$ that satisfy the specified boundary conditions. As we can continuously follow the value of θ from $\tau = 0$ to $\tau = L_\tau$, its actual value, and not just the angle modulo 2π, becomes significant; so we allow for an overall phase winding by $2\pi p$ in the boundary conditions. This boundary condition is the only remnant of the periodicity of the original lattice problem as $\theta(\tau)$ is allowed to assume all real values. We have also absorbed an overall normalization factor into the definition of the functional integral, and we will therefore not keep track of additive nonuniversal constants to the free energy such as E_0 of Section 5.5.

We now assert that $\mathcal{Z}_c$ and H_c are the universal scaling theories of H and $\mathcal{Z}$ in (6.16) and (6.17). Hence if we started with a different microscopic model, its universal properties would also be described by $\mathcal{Z}_c$, with the only change being in the values of ξ and $\tilde{h}$. For instance if we had a Hamiltonian like (6.16), but with jth neighbor interactions K_j, its continuum limit would also be H_c, with the same value for $\tilde{h}$, but ξ modified to

$$\xi = 2a \sum_{j=1}^{\infty} K_j j^2. \tag{6.25}$$

This continuum limit is valid for all models in which the summation over j in (6.25) converges. The universality of H_c also applies to models in which the constraint $\mathbf{n}_i^2 = 1$ is not imposed rigidly and fluctuations in the amplitude of $\mathbf{n}_i$ are allowed about their mean value. The prescription for determining the input value of ξ is however still very simple: Set the magnitude of $\mathbf{n}_i$ to its optimum value and measure the energy change of a uniform twist. Corrections due to the fluctuations in the magnitude of $\mathbf{n}_i$ about this optimum value will not modify the universal scaling theory (6.23).

Before turning to an evaluation of $\mathcal{Z}_c$ and its associated correlators, let us describe the scaling forms expected in the universal theory. These can be deduced by simple dimensional analysis. In the present case ξ, L_τ, and $\tilde{h}$ are the large lengths of the theory, and we simply make the appropriate dimensionless combinations. We thus have for the free energy $\mathcal{F} = -(\ln \mathcal{Z}_c)/L_\tau$

and the two-point correlator:

$$\begin{aligned} \mathcal{F} &= \frac{1}{L_\tau}\Phi_{\mathcal{F}}\left(\frac{L_\tau}{\xi}, \tilde{h}L_\tau\right), \\ \langle \mathbf{n}(\tau)\cdot\mathbf{n}(0)\rangle &= \Phi_n\left(\frac{\tau}{L_\tau}, \frac{L_\tau}{\xi}, \tilde{h}L_\tau\right), \end{aligned} \tag{6.26}$$

where $\Phi_{\mathcal{F}}$ and Φ_n are universal functions, portions of which will be determined explicitly below.

Let us evaluate $\mathcal{Z}_c$ in zero field ($\tilde{h} = 0$). To satisfy the boundary conditions let us decompose

$$\theta(\tau) = \frac{2\pi p\tau}{L_\tau} + \theta'(\tau), \tag{6.27}$$

where $\theta'(\tau)$ satisfies periodic boundary conditions $\theta'(L_\tau) = \theta'(0)$. Inserting this into (6.22) we find that the cross term between the two pieces of $\theta(\tau)$ vanishes because of the periodic boundary conditions on θ', and (6.24) becomes

$$\begin{aligned} \mathcal{Z}_c(\tilde{h}=0) = &\left(\sum_{p=-\infty}^{\infty} \exp\left(-\frac{\pi^2 p^2 \xi}{L_\tau}\right)\right) \\ &\times \int_{\theta'(L_\tau)=\theta'(0)} \mathcal{D}\theta'(\tau) \exp\left(-\frac{\xi}{4}\int_0^{L_\tau} d\tau \left(\frac{d\theta'}{d\tau}\right)^2\right). \end{aligned} \tag{6.28}$$

Now notice that the last functional integral is simply the familiar Feynman path integral for the amplitude of a single quantum mechanical free particle, of mass $\xi/2$ with coordinate θ', to return to its starting position after imaginary time L_τ. Using the standard expression for this we find finally

$$\mathcal{Z}_c(\tilde{h}=0) = (2\pi)\left(\frac{\xi}{4\pi L_\tau}\right)^{1/2} A(\pi\xi/L_\tau), \tag{6.29}$$

where the factor of 2π comes from the integral over $\theta'(0)$, and $A(y)$ is the elliptic theta function defined by

$$A(y) = \sum_{p=-\infty}^{\infty} e^{-\pi p^2 y}. \tag{6.30}$$

This result is clearly consistent with the scaling form for the free energy density $\mathcal{F} = -(\ln \mathcal{Z}_c)/L_\tau$ in (6.26).

Let us push the analogy with the quantum mechanics of a particle a bit further and complete the quantum–classical mapping by obtaining an explicit expression for the quantum Hamiltonian, H_Q, which describes the

scaling limit. Note that $\mathcal{Z}_c$ in (6.24), with the summation over p included, can be interpreted as the Feynman path integral of a particle constrained to move on a *circle* of unit radius; the angular coordinate of the particle is θ, and p represents the number of times the particle winds around the circle in its motion from imaginary time $\tau = 0$ to $\tau = L_\tau$. The term proportional to $\tilde{h}$ is then a potential energy term that preferentially locates the particle at $\theta = 0$. The Hamiltonian of this quantum particle is then

$$H_Q = -\Delta \frac{\partial^2}{\partial \theta^2} - \tilde{h} \cos\theta, \tag{6.31}$$

where, as we will see shortly, Δ is defined as in the Ising case to be the gap of H_Q in zero external field. As the mass of the quantum particle is $1/(2\Delta)$, we have by comparing with (6.22)

$$\Delta = \frac{1}{\xi}. \tag{6.32}$$

This is precisely of the form (5.49), and it is another realization of the fact that the gap of the quantum model is equal to the correlation "length" of the classical model along the imaginary time direction. For some of our subsequent discussion it is useful to express H_Q solely in terms of quantum operators. Let $\hat{\mathbf{n}}$ be the Heisenberg operator corresponding to $\mathbf{n}$. Let us also define $\hat{L}$ as the angular momentum operator of the rotor:

$$\hat{L} = \frac{1}{i} \frac{\partial}{\partial \theta}. \tag{6.33}$$

Then we have the commutation relation

$$[\hat{L}, \hat{n}_\alpha] = i \epsilon_{\alpha\beta} \hat{n}_\beta, \tag{6.34}$$

where α, β extend over the two coordinate axes, x, y in the spin plane, and $\epsilon_{xy} = -\epsilon_{yx} = 1$, with other components zero. These are precisely the $N = 2$ case of the commutation relations following from (1.17) and (1.20). The Hamiltonian H_Q is clearly

$$H_Q = \Delta \hat{L}^2 - \tilde{\mathbf{h}} \cdot \hat{\mathbf{n}}, \tag{6.35}$$

which is simply the quantum rotor model (1.22) in the presence of field $\tilde{\mathbf{h}}$, $1/(2\Delta)$ is the moment of inertia of the rotor, and commutation relation (6.34) is the $N = 2$ analog of (1.21). We have established the needed result: The scaling limit of the $D = 1$ classical XY ferromagnet is given exactly by the Hamiltonian of a single O(2) quantum rotor.

The Hamiltonian H_Q is related to the transfer matrix $\hat{T}$ (in (6.19)) of the

lattice XY model by a relationship identical to that found in (5.47). By a gradient expansion of (6.19) the reader can verify that

$$\hat{T} \approx \exp(-aH_Q) \tag{6.36}$$

to leading order in the lattice spacing a. So again, the transfer matrix "evolves" the system by an imaginary time a.

We can use the quantum–classical mapping and obtain explicit expressions for the universal scaling functions of the classical problem in (6.26). First, using the mapping (2.5) $T = 1/L_\tau$, let us write down the scaling forms (6.26) in the quantum language:

$$\begin{aligned} \mathcal{F} &= T\Phi_{\mathcal{F}}\left(\frac{\Delta}{T}, \frac{\tilde{h}}{T}\right), \\ \langle \mathbf{n}(\tau)\cdot\mathbf{n}(0)\rangle &= \Phi_n\left(T\tau, \frac{\Delta}{T}, \frac{\tilde{h}}{T}\right). \end{aligned} \tag{6.37}$$

We see here a structure that was used in (5.55), and which shall be used throughout the book. We characterize the universal properties by the "small" energy scales Δ, $\tilde{h}$ (these are the analogs of the "large" length scales of the corresponding classical problem, while the nonuniversal behavior at "small" length scales in the classical system maps onto high energy physics in the quantum system, which is not of interest here). These "small" energy scales then appear in universal scaling functions of dimensionless ratio of these energies with the physical temperature, T.

Let us turn to the evaluation of the scaling functions. The eigenstates, $\psi_\mu(\theta)$, and eigenvalues, ϵ_μ, of H_Q are determined by solving the Schrödinger equation

$$H_Q\psi_\mu(\theta) = \epsilon_\mu\psi_\mu(\theta) \tag{6.38}$$

subject to the boundary condition $\psi_\mu(0) = \psi_\mu(2\pi)$. The equation (6.38) can be considered as the continuum scaling limit of the eigenvalue equation (6.20), with the correspondence in (6.36) and $\lambda_\mu = \exp(-a\epsilon_\mu)$. The continuum limit partition function $\mathcal{Z}_c$ can be expressed directly in terms of H_Q:

$$\begin{aligned} \mathcal{Z}_c &= \mathrm{Tr}\exp(-H_Q/T) \\ &= \sum_\mu \exp(-\epsilon_\mu/T), \end{aligned} \tag{6.39}$$

where $T = 1/L_\tau$. The two-point correlator of $\hat{n}$ can also be expressed in the

quantum language

$$\langle \mathbf{n}(\tau)\cdot\mathbf{n}(0)\rangle = \frac{1}{\mathcal{Z}_c}\mathrm{Tr}\left(e^{-H_Q/T}e^{H_Q\tau}\hat{\mathbf{n}}e^{-H_Q\tau}\cdot\hat{\mathbf{n}}\right)$$
$$= \frac{1}{\mathcal{Z}_c}\sum_{\mu,\nu}|\langle\mu|\hat{\mathbf{n}}|\nu\rangle|^2 e^{-\epsilon_\mu/T}e^{-(\epsilon_\nu-\epsilon_\mu)\tau}, \tag{6.40}$$

where the summation over μ,ν extends over all the eigenstates of H_Q, and we have assumed $\tau > 0$.

The solution of (6.38), combined with (6.39) and (6.40), provides the complete solution of the universal scaling properties of the classical XY chain. An elementary solution of the eigenvalue equation (6.38) is only possible at $\tilde{h} = 0$, to which we will restrict our attention from now on. In zero field, the eigenstates are $\psi_m(\theta) \propto e^{im\theta}$, where m is an arbitrary integer, and the corresponding eigenvalues are Δm^2 (these are the states of (1.23)). The ground state has zero energy ($m = 0$), and, as promised, the gap to the lowest excited states ($m = \pm 1$) is Δ. We can therefore evaluate the partition function

$$\mathcal{Z}_c(\,\tilde{h}=0) = \sum_{m=-\infty}^{\infty}\exp\left(-\frac{\Delta m^2}{T}\right)$$
$$= A(\Delta/\pi T), \tag{6.41}$$

a result that satisfies (6.37); the function $A(y)$ was defined in (6.30). If we compare this with (6.29), and use (6.32) and (5.49), the equivalence of the two expressions for $\mathcal{Z}_c$ is not immediately obvious. However, equality can be established by use of the following inversion identity, which the reader is invited to establish as a simple application of the Poisson summation formula:

$$A(y) = \frac{A(1/y)}{\sqrt{y}}. \tag{6.42}$$

In terms of the original classical model, the expression (6.29) for $\mathcal{Z}_c$ is useful for large ξ (or large values of K, corresponding to a low classical "temperature," which has been absorbed into the definition of K) when its series converges rapidly; conversely the dual expression (6.41) is most useful for small ξ (or small K and high classical "temperatures").

Let us also discuss the form of the correlation functions at $\tilde{h} = 0$. Recalling (6.15), and the wavefunction $\psi_m(\theta) \propto e^{im\theta}$, we have the very simple matrix element

$$|\langle m|\hat{\mathbf{n}}|m+1\rangle|^2 = 1 \tag{6.43}$$

and all others vanish; the correlation function follows simply from (6.40), and it is clear that the result agrees with (6.37). In particular, at $T = 0$ or $L_\tau = \infty$ we have

$$\langle \mathbf{n}(\tau) \cdot \mathbf{n}(0) \rangle = e^{-\Delta|\tau|}, \tag{6.44}$$

which establishes, as in the Ising chain, the inverse of the gap Δ as the correlation length of the classical chain.

6.4 The classical Heisenberg chain and an O(3) quantum rotor

We now generalize the results of the previous section to the $D = 1$, $N = 3$ case. The $N = 3$ classical ferromagnet is also known as the classical Heisenberg chain. The partition function is still given by (6.13) and the classical Hamiltonian by (6.14), with the only change being that $\mathbf{n}$ is now a three-component unit vector. Taking its continuum limit as for $N = 2$ we replace (6.22) and (6.24) by the partition function

$$\begin{aligned} \mathcal{Z}_c &= \int \mathcal{D}\mathbf{n}(\tau)\delta(\mathbf{n}^2 - 1) \exp\left(-H_c[\mathbf{n}(\tau)]\right), \\ H_c[\mathbf{n}(\tau)] &= \int_0^{L_\tau} d\tau \left[\frac{(N-1)\xi}{4} \left(\frac{d\mathbf{n}(\tau)}{d\tau} \right)^2 - \tilde{\mathbf{h}} \cdot \mathbf{n} \right], \end{aligned} \tag{6.45}$$

with $\mathbf{n}(0) = \mathbf{n}(L_\tau)$; now $\xi = 2Ka/(N-1)$ and $\tilde{\mathbf{h}} = \mathbf{h}/a$ as in (6.23). We have chosen the definition of ξ by anticipating a later computation in which ξ will be seen to be the correlation length. We will only consider the case $N = 3$ in this subsection and have quoted, without proof, the form for general N; notice that (6.45) agrees with (6.22) for $N = 2$. Unlike (6.22), it is not possible to evaluate the partition function (6.45) in this form. Recall that for the $N = 2$ case of (6.22) we had a simple angular parameterization in which H became purely quadratic in the angular variable. One could parameterize the three-component $\mathbf{n}$ using spherical coordinates, but the resulting H is not simply quadratic.

Further progress toward the evaluation of $\mathcal{Z}_c$ can however be made after the quantum–classical mapping. To do this, note, as in (6.28), that the functional integral in (6.45) can be interpreted as the imaginary-time Feynman path integral for a particle moving in a three-dimensional space with coordinate $\mathbf{n}$. Then the term with $(\partial\mathbf{n}/\partial\tau)^2$ is its kinetic energy and its mass is $1/\xi$, and the term proportional to $\tilde{\mathbf{h}}$ is like a "gravitational potential energy." The constraint that $\mathbf{n}^2 = 1$ may be viewed as a very strong potential that prefers the particle move on the surface of a unit sphere. We can

therefore perform the quantum–classical mapping simply by writing down the Schrödinger Hamiltonian, H_Q, for this particle. The restriction that the motion take place on the surface of a sphere simply means that the radial kinetic energy term of the particle should be dropped. The resulting H_Q generalizes (6.35) to $N = 3$:

$$H_Q = \frac{\Delta}{2}\hat{\mathbf{L}}^2 - \tilde{\mathbf{h}} \cdot \mathbf{n}, \tag{6.46}$$

where the angular momentum operator $\hat{\mathbf{L}}$ has three components (in general it has $N(N-1)/2$ components); again this is simply the $N = 3$ single rotor model H_K in (1.22) in the presence of a field $\tilde{\mathbf{h}}$. The operators $\hat{\mathbf{L}}$ and $\hat{\mathbf{n}}$ obey the commutation relations in (1.21). The parameter Δ is again the energy gap at $\tilde{\mathbf{h}} = 0$, as we will see below, and is given by $\Delta = 1/\xi$, as in (6.32). If we determine all the eigenvalues ϵ_μ of H_Q then the explicit expression for $\mathcal{Z}_c$ is given by (6.39). Determination of the eigenvalues of H_Q can, for instance, be done by solving the Schrödinger differential equation for a wavefunction $\psi_\mu(\mathbf{n})$ on the surface of a unit sphere. The Hamiltonian in Schrödinger's equation is given by H_Q, with $\hat{\mathbf{L}}$ a differential operator:

$$L_\alpha = -i\epsilon_{\alpha\beta\gamma} n_\beta \frac{\partial}{\partial n_\gamma}. \tag{6.47}$$

In summary, the complete solution of the classical partition function $\mathcal{Z}_c$ is given by mapping the problem to the dynamics of a O(3) quantum rotor with Hamiltonian H_Q defined by Equations (2.69), (1.19), and (2.70), where the value of $\mathcal{Z}_c$ is given by (6.39).

We conclude this section by explicitly determining the eigenvalues for $\tilde{\mathbf{h}} = 0$. In this case, it is evident that the eigenfunctions ψ_μ are simply the spherical harmonics, and the eigenvalues are

$$(\Delta/2)\ell(\ell+1), \quad \ell = 0, 1, 2 \ldots \infty \tag{6.48}$$

with degeneracy $2\ell + 1$ (as in (1.24)), so that

$$\begin{aligned} \mathcal{Z}_c(\tilde{\mathbf{h}} = 0) &= \mathrm{Tr} e^{-H_Q/T} \\ &= \sum_{\ell=0}^{\infty} (2\ell+1) \exp\left(-\frac{\Delta}{2T}\ell(\ell+1)\right), \end{aligned} \tag{6.49}$$

replacing (6.41), and as before $T = 1/L_\tau$. The ground state is the nondegenerate $\ell = 0$ state, and it can be checked that the energy gap is Δ. The correlations continue to obey (6.44), and so there is no long-range order in the classical Heisenberg chain, and the correlation length $= 1/\Delta$.

6.5 Mapping to classical field theories

Continuing our analysis parallel to that of the Ising model in Section 5.6, here we will apply the result of Sections 6.3 and 6.4 to obtain a representation of the original d-dimensional quantum rotor model (6.1) as a classical statistical mechanics model in D dimensions.

Here our analysis is actually simpler than that in Section 5.6 because we can keep the imaginary time co-ordinate τ continuous at all stages. For the Ising model, we were forced to discretize time into M_τ steps of size a: this is because the Ising spins could only evolve in discrete steps. Here, we are dealing with continuous spin variables which can evolve in continuous time, and so the limit $a \to 0$ can be taken at the outset.

As in Section 5.6, we begin with the d-dimensional quantum rotor model, and then apply the results of Sections 6.3 and 6.4 independently to the quantum rotor on each site i. In particular, using the equivalence between (6.22) and (6.31) for $N = 2$, and that between (6.45) and (6.46) for general N, we can now write

$$\begin{aligned} \mathcal{Z} &= \mathrm{Tr} \exp\left(-H_R/T\right) \\ &= \prod_i \int \mathcal{D}\mathbf{n}_i(\tau) \delta(\mathbf{n}_i^2(\tau) - 1) \exp(-\mathcal{S}_n), \\ \mathcal{S}_n &= \int_0^{1/T} d\tau \left[\frac{1}{2J\tilde{g}} \sum_i \left(\frac{d\mathbf{n}_i(\tau)}{d\tau} \right)^2 - J \sum_{\langle ij \rangle} \mathbf{n}_i \cdot \mathbf{n}_j \right], \end{aligned} \tag{6.50}$$

along with the periodic boundary conditions $\mathbf{n}_i(1/T) = \mathbf{n}_i(0)$. This expression is of the needed form: it involves a summation over the orientation of a 'classical' O(N) spin located on a $D+1$-dimensional spacetime, with the temporal direction having the form of a circle of circumference $1/T$, *i.e.* the spacetime has the topology of a cylinder. After discretizing the time direction, it takes the form of the model (3.2) considered in Chapter 3, although we will not need to take that step here. A complementary mapping is obtained by taking the spatial continuum limit of (6.50): then we obtain the D-dimensional O(N) non-linear sigma model in (2.12), with c given in (6.11) and the coupling g given by

$$g = N\sqrt{\tilde{g}} a^{d-1}. \tag{6.51}$$

Finally, we can apply the arguments of Chapter 3 to motivate the D-dimensional model of the field ϕ_α ($\alpha = 1 \ldots N$) given by (2.11) or (3.26). Just as was the case in Chapters 3 and 4, the quantum field theory in (2.11) will be the most convenient formulation to understand the behavior of the quantum Ising and rotor models across the quantum critical point.

6.6 Spectrum of quantum field theory

We have finally assembled all ingredients to describe the quantum phase transition in the quantum Ising and rotor models. We have argued that the quantum field theory (2.11) completely describes all low energy properties in the vicinity of the quantum critical point: in particular it captures the excitations of both phases and of the critical point.

Having used the classical analysis of Chapters 3 and 4 to motivate the 'soft-spin' ϕ_α continuum formulation in (2.11), let us now work backwards from this classical theory to a Hamiltonian description in terms of a continuum quantum model. This will be a convenient way of describing the ground state and its excitations. Just as was the case for the classical model, we can analyze the continuum quantum model perturbatively in powers of the coupling u. As argued in Chapter 4 we can expect this perturbative computation to fail at the quantum critical point for $D < 4$, and we will then have to invoke the renormalization group analysis for a complete picture. However, in this section we will be satisfied by the mean-field description at lowest order in u: as we saw in Chapter 3, this gives an adequate description of both phases and of the critical point, failing mainly in the values of the critical exponents for $D < 4$.

Applying the arguments used to obtain (6.50) in reverse, we conclude that (2.11) is equivalent to the continuum quantum model with the Hamiltonian

$$\mathcal{H} = \int d^d x \left\{ \frac{1}{2} \left[\pi_\alpha^2 + c^2 (\nabla_x \phi_\alpha)^2 + r \phi_\alpha^2(x) \right] + \frac{u}{4!} \left(\phi_\alpha^2(x) \right)^2 \right\}. \tag{6.52}$$

Here $\pi_\alpha(x,t)$ is the canonical momentum to the field ϕ_α, which therefore satisfy the equal-time commutation relations

$$[\phi_\alpha(x), \pi_\beta(x')] = i \delta_{\alpha\beta} \delta(x - x'). \tag{6.53}$$

The remainder of this section analyzes the theory defined by (6.52) and (6.53), to leading order in u. Our analysis will be the quantum analog of the classical considerations in Section 3.2.

6.6.1 Paramagnet

First, let us consider the paramagnetic phase, $r > 0$. The effective potential has a minimum near $\phi_\alpha = 0$, and so the low-lying excitations will be small fluctuations of ϕ_α about this minimum. For these, we can ignore the quartic u term. Then (6.52) becomes a harmonic theory, which we can diagonalize into normal modes just as we did earlier for (6.7). Now the normal mode

expansion in terms of harmonic oscillator operators is

$$\begin{aligned}\phi_\alpha(x) &= \int \frac{d^dk}{(2\pi)^d}\frac{1}{\sqrt{2\varepsilon_k}}\left(a_\alpha(k)e^{i\vec{k}\cdot\vec{x}} + a_\alpha^\dagger(\vec{k})e^{-i\vec{k}\cdot\vec{x}}\right),\\ \pi_\alpha(x) &= -i\int \frac{d^dk}{(2\pi)^d}\sqrt{\frac{\varepsilon_k}{2}}\left(a_\alpha(\vec{k})e^{i\vec{k}\cdot\vec{x}} - a_\alpha^\dagger(\vec{k})e^{-i\vec{k}\cdot\vec{x}}\right),\end{aligned} \tag{6.54}$$

where the creation and annihilation operators satisfy the analog of the commutation relations in (6.9)

$$\begin{aligned}\left[a_\alpha(\vec{k}), a_\beta^\dagger(\vec{k}')\right] &= \delta_{\alpha\beta}(2\pi)^d\delta^d(\vec{k}-\vec{k}'),\\ \left[a_\alpha(\vec{k}), a_\beta(\vec{k}')\right] &= 0.\end{aligned} \tag{6.55}$$

Again, these commutation relations ensure that (6.53) is obeyed, and the Hamiltonian is just the sum of harmonic oscillators as in (6.10):

$$\mathcal{H} = \int \frac{d^dk}{(2\pi)^d}\varepsilon_k\left[a_\alpha^\dagger(\vec{k})a_\alpha(\vec{k}) + 1/2\right]. \tag{6.56}$$

The energy of these normal modes is

$$\varepsilon_k = (c^2k^2 + r)^{1/2}. \tag{6.57}$$

So our main result is that the low-lying excitations of the paramagnetic phase consist of N particles, which transform under the fundamental representation of O(N). This spectrum is seen to be in perfect correspondence with earlier results from the $g \gg 1$ expansions. For the $N = 1$ case, the particle in Section 5.2.1 is equivalent to the present excitations: both are created by the action of the order parameter $\phi_\alpha \sim \hat{\sigma}^z$ on the ground state. For $N > 1$, we have the N-fold degenerate particles discussed in Section 6.1.

The energy gap above the paramagnetic state, from (6.57), is $\Delta = \sqrt{r}$. Unlike our previous $g \gg 1$ analysis, we can now follow the evolution of this gap all the way up to the quantum critical point at $r = 0$. This gap vanishes at the critical point as in (1.1), thus identifying the mean-field exponent $z\nu = 1/2$. Recall, that we noted earlier in Section 2.1 that the quantum Ising and rotor models have dynamic exponent $z = 1$.

6.6.2 Quantum critical point

Right at the critical point $r = 0$, we have our first result for the nature of the excitation spectrum: there are N particles, all dispersing as

$$\varepsilon_k = ck \tag{6.58}$$

The linear dispersion is consistent with dynamic exponent $z = 1$. It should be contrasted with small momentum $\sim k^2$ dispersion of particles in the paramagnetic phase in (6.57). We will see in Chapter 7 that the particles are not stable excitations of the critical point for $D < 4$: the strong interactions from the quartic coupling u makes them susceptible to decay into multiple lower energy excitations, and the quasiparticle residue Z is equal to zero at the quantum critical point. In contrast, the particles in (6.57) are stable in the paramagnetic phase, with a non-zero Z.

6.6.3 Magnetic order

For $r < 0$, just as in Section 3.2, the potential in (6.52) is minimized at $\phi_\alpha = N_0 \delta_{\alpha,1}$, where N_0 was given in (3.23)

$$N_0 = \sqrt{\frac{-6r}{u}}. \tag{6.59}$$

We have arbitrarily chosen the magnetic order oriented along the $\alpha = 1$ direction, without loss of generality. Now let us write

$$\phi_\alpha(x) = N_0 \delta_{\alpha,1} + \tilde{\phi}_\alpha(x) \tag{6.60}$$

and expand the Hamiltonian in (6.52) to quadratic order in the $\tilde{\phi}_\alpha$. A straightforward computation yields

$$\mathcal{H} = \frac{1}{2} \int d^d x \left\{ \sum_{\alpha=1}^{N} \left(\pi_\alpha^2 + c^2 (\nabla_x \tilde{\phi}_\alpha)^2 \right) + 2|r| \tilde{\phi}_1^2 \right\}. \tag{6.61}$$

We can now quantize just as in Section 6.6.1, and find 2 types of excitations:

$$\begin{array}{ccc} \varepsilon_k = ck & , & N-1 \text{ particles;} \\ \varepsilon_k = (c^2 k^2 + 2|r|)^{1/2} & , & 1 \text{ particle.} \end{array} \tag{6.62}$$

The gapless $N - 1$ particles are easy to identify: they are clearly the spin waves we met in Section 6.2 in (6.11).

For $N > 1$, the single particle with energy gap $\sqrt{2|r|}$ is not one we have met before. It corresponds to small longitudinal oscilations of the ϕ_1 field about the minimum at $\phi_1 = N_0$. See Fig 6.1. It is the analog of what is known in the particle theory literature as the Higgs particle. In general, this Higgs particle can decay into multiple lower-energy spin waves. It has been argued that such decay processes dominate for $d < 3$, and the Higgs particle is therefore not a stable excitation. However, in $d = 3$, the Higgs is stable; indeed neutron scattering experiments [420] on $TlCuCl_3$ have observed the Higgs excitation [436]. See Fig 6.2.

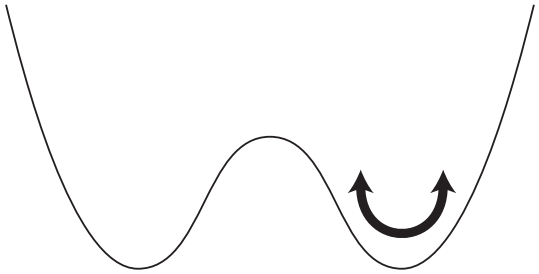

Figure 6.1 The longitudinal mode corresponding to the oscillations of ϕ about the non-zero minimum value. There are also $N-1$ gapless transverse modes which move orthogonal to the plane of the page which are not shown.

For $N = 1$, we have only the particle excitation with the energy gap $\sqrt{2|r|}$. For $d > 1$, we claim this is the same as the low-lying particle excitation found in Section 5.3.1 in the small g expansion. In the latter approach, the excitation was a 'bubble' of a down spin moving in a ferromagnetic background of up spins. In the present field-theoretical analysis we have fluctuations of ϕ_1 about N_0, which also contribute to decrease in the local ferromagnetic moment.

Finally, what about the case $N = 1$, $d = 1$? We found in the small g expansion in Section 5.3.2 that the stable excitations were domain walls or 'kinks' that interpolated between the ground states with magnetization $\pm N_0$. Here, such a domain wall involves interpolating ϕ_1 between the minima in the effective potential at $\pm N_0$, over the maximum at $\phi_1 = 0$. See Fig 6.3. This domain wall is also a local minimum of the potential in the Hamiltonian but with a space-dependent $\phi_1(x)$. Indeed, taking the variational derivative of (6.52) with respect to variations in $\phi_1(x)$, we obtain the saddle-point equation

$$-\partial_x^2\phi_1 - |r|\phi_1 + u\phi_1^3/6 = 0. \tag{6.63}$$

This equation has the usual solutions $\phi_1 = \pm N_0$, but also the space-dependent solution

$$\phi_1(x) = \pm N_0 \tanh\Big((x - x_0)\sqrt{|r|}/2\Big), \tag{6.64}$$

where x_0 is abitrary. This is the domain wall centered at $x = x_0$. Quantization of the motion of x_0 leads to the domain wall particle. The Higgs particle of small ϕ_1 oscillations about $\pm N_0$ is evidently unstable to decay into a pair of domain wall particles: we discussed this phenomenon in Section 5.3.2. We will study these domain walls more completely in Chapter 10, where we

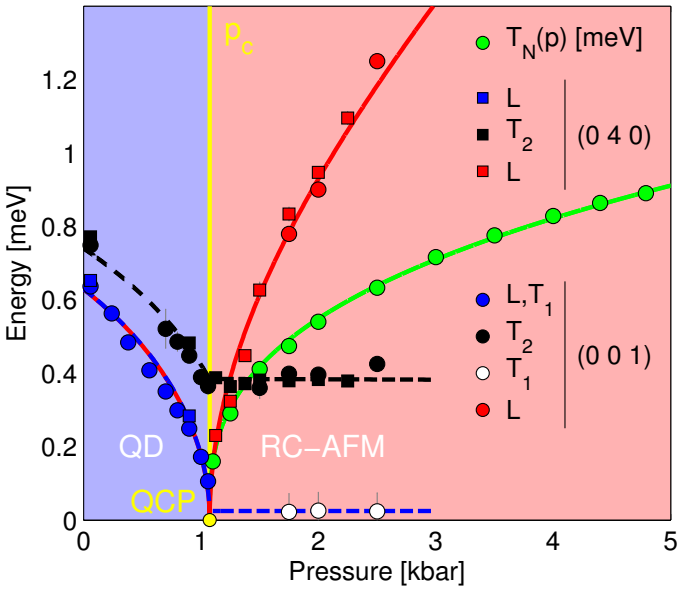

Figure 6.2 From Ref. [420]. Measurements of the excitation energies in $TlCuCl_3$ across the quantum critical point induced by applied pressure (horizontal axis). This transition is described by the O(3) quantum rotor model in $d = 3$. Below the critical pressure, we are in the paramagnetic phase, and the 3 quasiparticle modes are shown as blue and black dots (split by spin-orbit effects not discussed here). Above the critical pressure, in the magnetically ordered phase, the 2 spin wave modes are shown by the blue and black dots. However there is also an additional Higgs mode shown by the red dots. The ratio of the energy of the Higgs mode to the triplet mode on the paramagnetic side is close to $\sqrt{2}$, as predicted [436] by the ratio of (6.57) and (6.62).

will find that they are fermions, and provide a complete description of the transition into the paramagnetic state.

Exercises

6.1 Establish the connection between the quantum rotor model of Section 1.4.2, and the spin ladder model described in Section 1.4.3. Note that the matrix elements of $\mathbf{n}_i$ in the angular momentum eigenstates are equal to those of the position operator between the spherical harmonics. Determine the spectrum of its angular momentum $\ell = 1$ excitations to leading order in g. By mapping this spectrum to that of the spin ladder, determine suitable values of K and g.

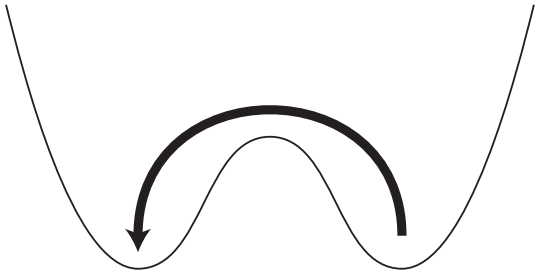

Figure 6.3 A domain wall between 2 Ising ferromagnetic states interpolates from one minimum of the effective potential to the other.

6.2 *O(2) rotors with long-range interactions:* An array of charged superconducting dots at the sites, i (with positions r_i) of a d-dimensional cubic lattice is described by the Hamiltonian

$$H = \sum_i \frac{\hat{n}_i^2}{2C} + \sum_{i<j} \hat{n}_i \hat{n}_j \frac{e^{*2}}{|r_i - r_j|} - J \sum_{\langle \alpha\alpha' \rangle} \cos\left(\hat{\phi}_i - \hat{\phi}_j\right) \tag{6.65}$$

where $\hat{n}_i$ is the number operator for Cooper pairs on dot i (each Cooper pair has charge $e^* = 2e$), $\hat{\phi}_i$ is the conjugate phase operators, and the only non-vanishing commutation relation is

$$\left[\hat{\phi}_i, \hat{n}_j\right] = i\delta_{\alpha\alpha'} \tag{6.66}$$

Assume we are in the large J superconducting phase where the phases are all aligned at $\hat{\phi}_i = 0$ (say). Obtain the Heisenberg equations of motion for $\hat{\phi}_i$ and $\hat{n}_i$, and linearize them for small fluctuations about the ground state. By determining the normal mode spectrum of these equations, obtain the long-wavelength form of the "plasmon" oscillations in $d = 1, 2, 3$.

6.3 Consider the two-particle sector of the quasiparticle excitations of the paramagnetic state described in Section 6.6.1. The particles have a two-body interaction proportional to u. Compute the matrix elements of this interaction $\langle k_1, \alpha_1 | u | k_2, \alpha_2 \rangle$. Set up the two-body scattering problem, and discuss qualitative features of the low momentum scattering amplitude in $d = 1, 2, 3$. Compare your results with those obtained in the $1/g$ expansion of the Ising model in exercise 5.5.2.